Growing Optimized Anisotropic Microstructures with Reaction/Diffusion

David-Henri Garnier, Martin-Pierre Schmidt, Damien Rohmer

Journées Françaises de l'Informatique Graphique 2021 / R.Vergne and N.Mellado.
(Paper Chairs)

Growing Optimized Anisotropic Microstructures with Reaction/Diffusion

D.H. Garnier[1], M.P. Schmidt[2] and D. Rohmer[1]

[1] LIX, Ecole Polytechnique/CNRS, IP Paris
[2] LMI, Normandie Univ., INSA Rouen

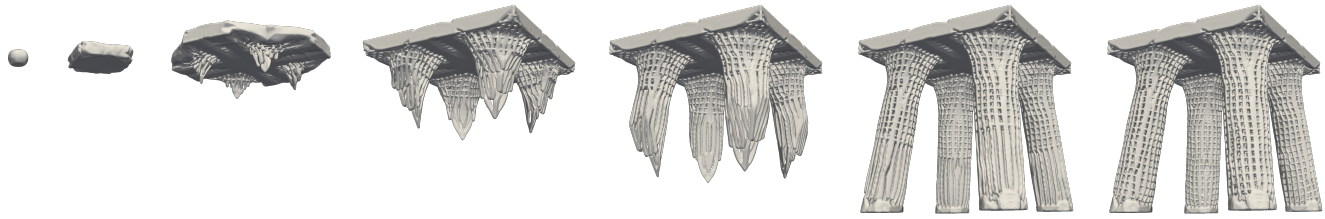

Figure 1: Growth of a lattice-like, stress-aligned, four-legged stool using our adapted Reaction/Diffusion-based approach.

Abstract

Lattice structures can present advantageous mechanical properties while remaining remarkably lightweight. Precise lattice design can however be tricky to set up on arbitrary domain with classical 3D modeling methods as it involves very fine oriented details. Interestingly, natural porous structures can present such lattice-like design which motivates the seek for bio-inspired approaches. In this paper we present a novel method to grow lattice-like structures within an arbitrary shape and aligned along an oriented field using adapted Reaction/Diffusion systems. While not directly computed from a global optimization process our structures still demonstrate remarkable structural properties for which we provide examples with numerical validation.

CCS Concepts

•***Computing methodologies*** → ***Shape modeling;*** *Volumetric models; Mesh models;*

1. Introduction

Recent advances in Additive Manufacturing and 3D Printing allows for high shape complexity that leads to seek for new lightweight designs. Hence there has been a growing interest in design of optimized multi-scale structures [LSZ*14, MDL16, DTZ17, MSDL17, WAWS18, LGC*18, ALSL*18, AK21, SOG*21]. Recent works are mostly built upon Topology Optimization [LHZ*18, PT08, GS18, SPG19, AGDP19, GSA*20, WSG21].

In the field of structural optimization, it is well known that the orientation of orthotropic microstructures has to be locally aligned with the principal stress directions for single-load case stiffness-optimal structure design [Mic04, Ped89, AK93, AJL*19]. Some natural materials show remarkable mechanical performances based on this stress orientation property [Woo60]. In this paper, we describe a novel bio-inspired method to design conforming lattice-like structures. Our method divides into two major steps. The first step proposes to generate intermediate structures with patterns oriented by an underlying tensor field and limited by a prescribed 3D shape with a growing process. This growth phase is controlled by an anisotropic Reaction/Diffusion model. The second step starts by applying some filter to the different structures to operate on the thickness of the oriented structures before combining them with Boolean operations in a similar way than [GDAP20].

Our contributions are the following:

- A general method for designing field conformal lattice-like structures, compatible with the workflow of topology optimization
- A novel approach based on a classic Reaction/Diffusion model to design global structure using anisotropic growth of microstructures
- A new multi-scale process to design optimized structures which constitute a good trade-off between stiffness property and resistance to buckling despite not being directly an optimizer of these properties

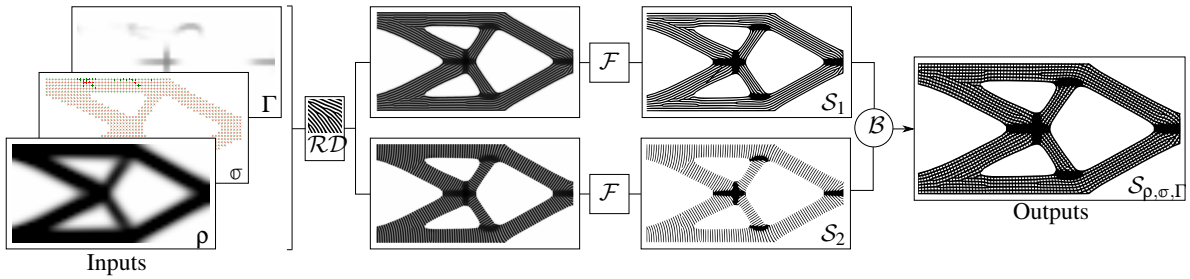

Figure 2: Global pipeline of our method. The first step ($\mathcal{RD}$) designates the Reaction/Diffusion, the intermediate step ($\mathcal{F}$) represents a filtering process while the final step ($\mathcal{B}$) is constituted of boolean operations

2. Method

2.1. Overview

Let us consider a rectangular domain Ω, subset of R^2 or R^3, representing the domain of definition of the three following fields used as inputs of our method as illustrated in Fig.2-left. First the scalar field $\rho(\mathbf{x} \in \Omega) \in [0,1]$, describes an initial notion of material density at each position in Ω. For a given isovalue $iso \in]0,1[$, the domain implicitly defined by $\rho(\mathbf{x}) > iso$ corresponds to the general appearance of the 3D shape where the micro-structure should be synthesized, and will be designated as *infill space*. Second, a *tensor field* $\varpi(\mathbf{x} \in \Omega)$ (for instance associated to the stress tensor), whose principal directions are considered to be the desired local orientation of the microstructures. Third, another scalar field $\Gamma(\mathbf{x} \in \Omega) \in [0,1]$ called *infill map* used to indicate the local regions to infill preferentially with solid material instead of lattice microstructures. All inputs and intermediate field values are stored on a discretized grid, and we may pre-process these inputs in up-sampling if needed their values by interpolation to any grid resolution adapted to our expected lattice microstructure.

The output of our approach is also described as a scalar field $\mathcal{S}_{\rho,\varpi,\Gamma}(\mathbf{x} \in \Omega) \in [0,1]$ shown Fig.2-right. The resulting shape surface is described as an isovalue of $\mathcal{S}$ which can be computed typically using marching cube or dual contouring when a triangular mesh is expected for visualization and manufacturing purpose. This surface represents an hybrid structure mostly filled with lattice aligned with both the tensor field directions and the boundary of the *infill space*. More precisely, at the boundary the lattice remains oriented according to the tensor field while shaped by the outer shell.

The core of our algorithm lies in the two major steps ($\mathcal{RD}$) and ($\mathcal{B}$). Step ($\mathcal{RD}$) is the actual anisotropic Reaction/Diffusion process allowing to synthesize intermediate scalar fields with locally oriented patterns. We compute 2 (resp. 3) independent processes in 2D (resp. 3D), while considering for each of them one of the principal tensor direction to be the main diffusion direction. The anisotropic Reaction/Diffusion patterns have a linear structure in 2D, and a surfacic one in 3D, and are restricted to grow in the regions specified by ρ as explained in Sec. 2.3. Once these intermediate fields are generated, the final lattice structure is generated in step ($\mathcal{B}$). To this end, we first apply a filter ($\mathcal{F}$) on each of the intermediate fields in order to steepen the variations of the field as well as thickening or thinning the patterns depending on their direction to optimize the mechanical structure associated to them. The output field $\mathcal{S}$ is finally obtained in combining the previous filtered fields using Boolean operations in order to generate a single lattice organization from the individual oriented patterns. These last steps are described in Sec. 2.4.

2.2. Inputs

This section describes with more details the automatic computation we followed to generate the input fields ρ, ϖ, Γ. While these fields can be provided using arbitrary methods, we will describe them as being automatically computed from a topology optimization as it provides an interesting case of application in the context of structural optimization.

Infill Space ρ. The purpose of this input density field is to design the overall shape which will be used as a boundary for lattice material infill. We adopt a simple approach where this boundary is defined by the optimal distribution of a budget of solid material maximizing the stiffness, given a fix design space with loads and constraints. Hence our desired input density field can be seen as the direct output of the classical compliance topology optimization problem subject to a global volume constraint, relying on the density-based method colloquially referred to as the *Solid Isotropic Material with Penalization* (SIMP) approach described by [BS99]. A numerical optimization on a low resolution grid can be conducted following [ACS*11]. The example used as input for Fig.2 is referred to as the *Cantilever* problem, a *de facto* standard test case in the litterature: a load is applied vertically in the middle of the right edge of the design space while the displacement is constrained all along the left edge.

Tensor field ϖ. The stress tensor field $\varpi(\mathbf{x} \in \Omega)$ can then be extracted from this preliminary optimization. For each element $\mathbf{x}$, the tensor is diagonalizable in an orthogonal basis with real eigenvalues called the principal stresses and their associated eigenvectors form a rotation matrix $\mathbb{R}(\mathbf{x})$ which characterizes the principal stress directions perpendicular to the planes where the principal stresses act.

Infill Map Γ. The Infill Map indicates the areas to infill with homogeneous material. It can be divided into two sub-maps: $\Gamma(\mathbf{x}) = (\Gamma_c \cup \Gamma_\varpi)(\mathbf{x}) = \max(\Gamma_c(\mathbf{x}), \Gamma_\varpi(\mathbf{x}))$. The first one $\Gamma_c(\mathbf{x})$ is given by the designer constraints and the other one $\Gamma_\varpi(\mathbf{x})$ is derived from the previous rotation field. This second map addresses an issue encountered when the input stress field is locally isotropic, or is associated

to very low values. In this case, the ordering and direction of the eigenvalues become meaningless, and the extracted rotation field would exhibit discontinuities. As there is no clear orientation to follow in these regions, we propose to infill them with plain material. To detect these regions, we propose an automatic computation assessing the local consistence of the alignment of all eigenvectors using the value $a(\mathbf{x}) = \frac{1}{|N(\mathbf{x})|d} \sum_{\mathbf{y}\in N(\mathbf{x})} \sum_{1\leq i\leq d} |\mathbf{v}_i(\mathbf{y}) \cdot \mathbf{v}_i(\mathbf{x})|$ with $N(\mathbf{x})$ the set of neighbours of the element situated in $\mathbf{x}$. We can then define $\Gamma_\varpi(\mathbf{x}) = (1 - a(\mathbf{x}))\rho(\mathbf{x})$.

2.3. Pattern Growth

The concept of Turing patterns was first introduced by Alan Turing [Tur52] in a foundational paper. The original theory explains pattern formation through a Reaction/Diffusion mechanism and as of this day it remains a major theory in theoretical biology used to model embryonic development as well as skin pigmentation. Here we are only interested in this model as a *tool* to generate smooth oriented patterns through the integration of a PDE. Hence the growth phase of our method is controlled by a two-species Reaction/Diffusion system which is a variant of the Gray-Scott model [GS84, Pea93] where the first species diffuses anisotropically. In this case the evolution of the concentrations $u(\mathbf{x},t)$ and $v(\mathbf{x},t)$ of the two reactive chemical species U and V is described by the following set of equations:

$$\begin{cases} \frac{\partial u}{\partial t} = \varpi(\mathbf{x})\nabla^2 u + \gamma f(u,v) \\ \frac{\partial v}{\partial t} = d\nabla^2 v + \gamma g(u,v) \end{cases} \tag{1}$$

where ϖ represent the anisotropic diffusion tensor, $d = \frac{D_v}{D_u}$ the diffusion ratio between the two species, and γ a parameter which controls the characteristic length of the pattern. In the original model the chemical U is added in the environment at a feed rate F while the chemical V is removed at a kill rate k. Both chemicals diffuse but U diffuses faster than V ($d < 1$) to observe patterns. The reaction kinetics is hence controlled by the following functions:

$$\begin{cases} f(u,v) = -uv^2 + F(1-u) \\ g(u,v) = uv^2 - (k+F)v \end{cases} \tag{2}$$

Pattern growth can be restricted to a design region $\Omega = \{\mathbf{x}, \quad \rho(\mathbf{x}) > s\}$ (for s chosen in $]0,1[$) by redefining the term $\gamma g(u,v)$ as

$$\gamma g(u,v)\mathbb{1}_\Omega - \lambda(1-\mathbb{1}_\Omega)v, \tag{3}$$

where $\mathbb{1}_\Omega(\mathbf{x})$ takes the value 1 if $\mathbf{x} \in \Omega$ and 0 otherwise. We set $\lambda > 0$ and $\lambda \gg F,k$ such that the species of interest $(1-U)$ (*i.e.* which will generate the intermediate oriented structures) is exponentially "killed" outside the area of interest. We also extend the value k to a space-varying field defined as $k(\mathbf{x}) = k\,(1 - \alpha\Gamma(\mathbf{x}))$. This allows increase the concentration of V (and so $(1-U)$) conformly to the *Infill Map*, while the parameter $\alpha \in [0,1]$ is used to adjusts how much these regions should be infilled.

Our objective is to generate a lattice structure from the synthesized patterns. To this end, we simulate d independent Reaction/Diffusion processes, with $d = \{2,3\}$ being the dimension of the embedding. Each process $i \in [1,d]$ uses its own diffusion tensor ϖ_i favouring one of the main direction of $\varpi = \mathbb{R}\mathbb{\Lambda}\mathbb{R}^T$ and defined by:

$$\varpi_i = \frac{1}{\mathrm{Tr}(\mathbb{D}_i)} \mathbb{R}\mathbb{D}_i\mathbb{R}^T \tag{4}$$

where $\mathbb{D}_i$ is a diagonal matrix filled with 1 on the diagonal and $\xi > 1$ the custom anisotropy at the (i,i) position. This will generate patterns oriented along each principal direction of the input tensor field. Gathering all together, each oriented intermediate structures $\mathcal{S}_i$ is represented by a (normalized) density field computed from the finite differences integration of each following system:

$$(\mathcal{S}_i) \begin{cases} \frac{\partial u_i}{\partial t} = \varpi_i(\mathbf{x})\nabla^2 u_i + \gamma f(u_i,v_i) \\ \frac{\partial v_i}{\partial t} = d\nabla^2 v_i + \gamma g(u_i,v_i)\mathbb{1}_\Omega - \lambda(1-\mathbb{1}_\Omega)v_i \\ f(u_i,v_i) = -u_i v_i^2 + F(1-u_i) \\ g(u_i,v_i) = u_i v_i^2 - [k\,(1-\alpha\Gamma(\mathbf{x})) + F]\,v_i \\ u_i(\mathbf{x},t=0) = 1, \quad \begin{cases} v_i(\mathbf{x}\in\mathcal{D}_0, t=0) = 1 \\ v_i(\mathbf{x}\notin\mathcal{D}_0, t=0) = 0 \end{cases} \end{cases} \tag{5}$$

where $\mathcal{D}_0$ designates the initial "seed", typically a small disk (in 2D) or sphere (in 3D) included in the *infill space*. This small initial seed was preferred to a large initial and possibly random covering of the infill space, as we noticed experimentally that the Reaction/Diffusion process generates more regular patterns when these are developed as growth through empty space. For the cantilever $\mathcal{S}_1$ and $\mathcal{S}_2$ can be seen Fig.2 (before and after filtering) as the result of an isosurface extraction of the density fields $s_i = 1 - u_i$.

2.4. Structure compilation

By merging the different substructures infilled with oriented patterns along the principal stress directions, it is possible to generate a shape with oriented lattice. A filter step is added to adapt the structure thickness before combining them. The result for the cantilever can be seen Fig.2-right.

Magnitude filter. [BK88] introduced the unit-cell with a rectangular hole as it constitutes an optimized microstructure compared to a regular square cell. Following this idea, in order to enhance the structural performance relatively to the mass, one can shift the iso to enlarge the pattern oriented along the first principal stress directions while reducing the width of the others. It can be achieved by redefining the density fields as follow

$$\tilde{s_i} = Normalize\left(\max\left(\min(s_i, s_{\varpi_i} + s_{w_{\varpi_i}}), s_{\varpi_i} - s_{w_{\varpi_i}}\right)\right) \tag{6}$$

where *Normalize* means that the density field is normalized between 0 and 1, s_{ϖ_i} denotes the targeted isovalue according to the direction i and $s_{w_{\varpi_i}}$ a parameter which applies a threshold favouring a binary structure while preserving its smoothness.

Boolean Operation. The final structure can be generated through the use of binary merging operators of implicit surfaces, corresponding to the use of min and max functions on their field values:

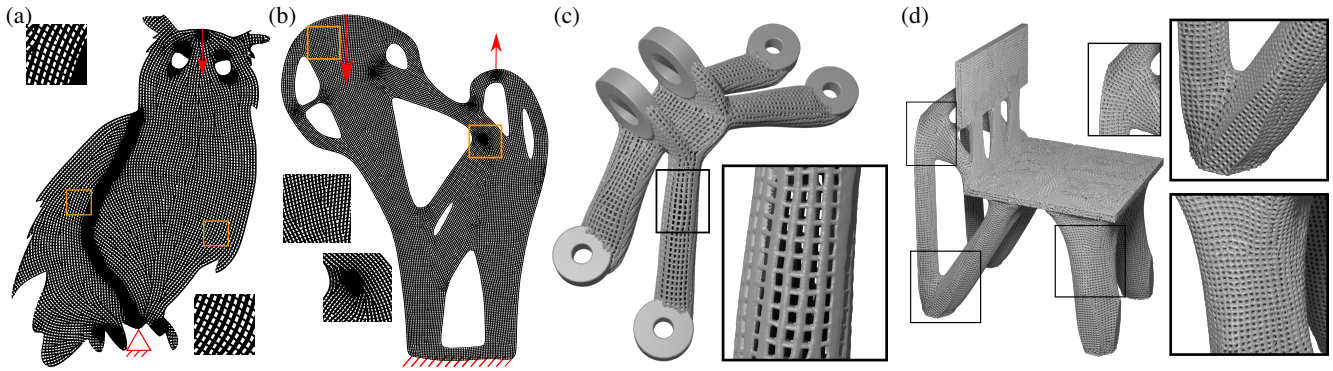

Figure 3: Different results with size of the grid: (a) Owl (752×1024) (b) Optimized Femur Head (2048×2624) (c) Lattice *GE Bracket* $(302 \times 512 \times 826)$ (d) Optimized lattice chair $(504 \times 360 \times 720)$

$$(\mathcal{S}) \begin{cases} \mathcal{S}_{2D} = \mathcal{S}_1 \cup \mathcal{S}_2 = \max(\tilde{s}_1, \tilde{s}_2) \\ \mathcal{S}_{3D} = \bigcup\limits_{i \neq j} \mathcal{S}_i \cap \mathcal{S}_j = \max\limits_{i \neq j} \left(\min\limits_{i \neq j} (\tilde{s}_i, \tilde{s}_j) \right) \end{cases} \tag{7}$$

3. Results and analysis

Fixed user-defined 2D shape: Owl. The first result Fig.3a is an example of structure generated from a pre-defined shape given by the designer. The input stress field is computed from topology optimization considering a fixed load and the final structure is generated by our method.

Optimized 2D shape: Femur Head. Fig.3b gives an example of a structure optimized inside the the overall shape of a femur head.

3D Optimized GE Bracket. Fig.3c shows our version for the *GE Bracket* scenario [Gra13] in case of a single load.

3D Optimized Chair. We propose to compare our result with the previous work from Wu et al. [WWG21] that proposed an optimized lattice chair generated using a Topology Optimization with oriented homogenized material followed by a parameterization optimization algorithm to design the lattice. Using the same underlying tensor field, the growth lattice obtained using our method is shown Fig.3d. Our result shows more lattice regularity especially near the surface of the object due to the aptitude of the Reaction/Diffusion to smoothly grow along the overall 3D shape.

Non-linear Structural Analysis. We run a general non-linear analysis in Abaqus 2021 to compare two design variants for the MBB Beam scenario and retrieve the force-displacement curves shown in Fig. 4. The two design variants have the same mass and are obtained with a classical compliance-based topology optimization (TO design) and with the proposed Reaction-Diffusion approach (RD design). The force-displacement curves of both design initially start with a roughly linear portion with the steeper slope indicating that the TO design achieves a higher stiffness, which is to be expected because it was specifically optimized for maximum stiffness. However, at a load magnitude of approximately 140 kN the TO design undergoes in-plane buckling and collapses. In contrast, the RD design shows near-linear deformation up to a load magnitude of 200 kN, and supports a peak load approximately 70% higher than the TO design.

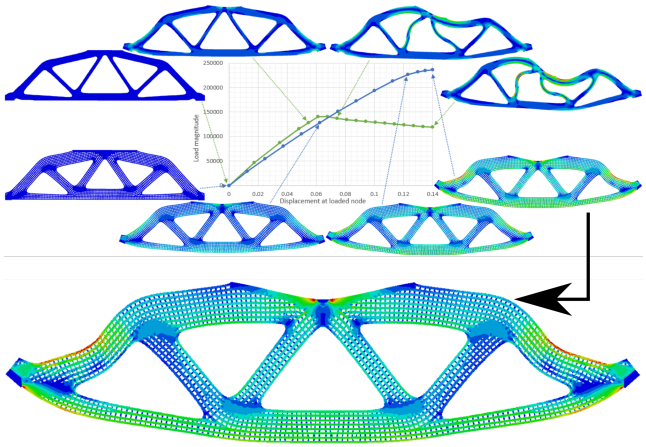

Figure 4: Force-Displacement curves for TO design variant (in green) and the RD design (in blue) in an MBB Beam scenario, with a zoom on RD design variant at peak load in the non linear analysis.

4. Conclusion

The present work proposed a novel approach to design conforming lattice-like structures, inspired by morphogenesis. Our method finds its main application in the design of optimized microstructures oriented by inputs which can be provided by a stress field or an anisotropic material orientation field inside a structurally optimized shape. In this context, our lattice-like structures come as a good trade-off between pure stiffness property and resistance to buckling despite they are not the output of an optimizer of these properties. Due to its multiscale nature, our method is fast and scalable to high resolution designs. Moreover, the microstructure generation is completely local, allowing the designer to dynamically interact with the growing structure, by erasing or modifying some parts and letting it evolve. Additionally, the aptitude of the Reaction/Diffusion to smoothly grow along the overall 3D shape ensure to generate structures with high lattice regularity, which is desirable both for aesthetics and mechanical performance considerations.

References

[ACS*11] ANDREASSEN E., CLAUSEN A., SCHEVENELS M., LAZAROV B. S., SIGMUND O.: Efficient topology optimization in matlab using 88 lines of code. *Structural and Multidisciplinary Optimization 43*, 1 (2011), 1–16. doi:10.1007/s00158-010-0594-7. 2

[AGDP19] ALLAIRE G., GEOFFROY-DONDERS P., PANTZ O.: Topology optimization of modulated and oriented periodic microstructures by the homogenization method. *Computers & Mathematics with Applications 78*, 7 (2019), 2197–2229. doi:10.1016/j.camwa.2018.08.007. 1

[AJL*19] ARORA R., JACOBSON A., LANGLOIS T. R., HUANG Y., MUELLER C., MATUSIK W., SHAMIR A., SINGH K., LEVIN D. I.: Volumetric michell trusses for parametric design & fabrication. In *Proceedings of the 3rd ACM Symposium on Computation Fabrication* (New York, NY, USA, 2019), SCF '19, ACM. doi:10.1145/3328939.3328999. 1

[AK93] ALLAIRE G., KOHN R. V.: Optimal design for minimum weight and compliance in plane stress using extremal microstructures. *European journal of mechanics. A. Solids 12*, 6 (1993), 839–878. 1

[AK21] AHSAN A. M. M. N., KHODA B.: Characterizing novel honeycomb infill pattern for additive manufacturing. *Journal of Manufacturing Science and Engineering 143*, 2 (2021), 021002. doi:10.1115/1.4048044. 1

[ALSL*18] ATTENE M., LIVESU M., S. LEFEBVRE T. F., RUSINKIEWICZ S., ELLERO S., MARTÍNEZ J., BERMANO A. H.: Design, representations, and processing for additive manufacturing. *Synthesis Lectures on Visual Computing: Computer Graphics, Animation, Computational Photography, and Imaging 10*, 2 (2018), 1–146. doi:10.2200/S00847ED1V01Y201804VCP031. 1

[BK88] BENDSØE M. P., KIKUCHI N.: Generating optimal topologies in structural design using a homogenization method. *Computer methods in applied mechanics and engineering 71*, 2 (1988), 197–224. doi:10.1016/0045-7825(88)90086-2. 3

[BS99] BENDSØE M. P., SIGMUND O.: Material interpolation schemes in topology optimization. *Archive of applied mechanics 69*, 9 (1999), 635–654. doi:10.1007/s004190050248. 2

[DTZ17] DONG G., TANG Y., ZHAO Y. F.: A survey of modeling of lattice structures fabricated by additive manufacturing. *Journal of Mechanical Design 139*, 10 (2017), 100906. doi:10.1115/1.4037305. 1

[GDAP20] GEOFFROY-DONDERS P., ALLAIRE G., PANTZ O.: 3-d topology optimization of modulated and oriented periodic microstructures by the homogenization method. *Journal of Computational Physics 401* (2020), 108994. doi:10.1016/j.jcp.2019.108994. 1

[Gra13] Grabcad ge jet engine bracket challenge., 2013. http:grabcad.com/challenges/ge-jet-engine-bracket-challenge.Accessed:2020-07-23. 4

[GS84] GRAY P., SCOTT S.: Autocatalytic reaction in the isothermal continuous stirred tank reactor. *Chemical engineering science 1* (1984), 1087–1097. doi:10.1016/0009-2509(84)87017-7. 3

[GS18] GROEN J. P., SIGMUND O.: Homogenization-based topology optimization for high-resolution manufacturable microstructures. *International Journal for Numerical Methods in Engineering 113*, 8 (2018), 1148–1163. doi:10.1002/nme.5575. 1

[GSA*20] GROEN J. P., STUTZ F. C., AAGE N., BÆRENTZEN J. A., SIGMUND O.: De-homogenization of optimal multi-scale 3d topologies. *Computer Methods in Applied Mechanics and Engineering 364* (2020), 112979. doi:10.1016/j.cma.2020.112979. 1

[LGC*18] LIU J., GAYNOR A. T., CHEN S., KANG Z., SURESH K., TAKEZAWA A., LI L., KATO J., TANG J., WANG C. C. L., CHENG L., LIANG X., TO A.: Current and future trends in topology optimization for additive manufacturing. *Structural and Multidisciplinary Optimization 57* (2018), 2457–2483. doi:10.1007/s00158-018-1994-3. 1

[LHZ*18] LIU H., HU Y., ZHU B., MATUSIK W., SIFAKIS E.: Narrow-band topology optimization on a sparsely populated grid. *ACM Transactions on Graphics (TOG) 37*, 6 (2018), 1–14. doi:10.1145/3272127.3275012. 1

[LSZ*14] LU L., SHARF A., ZHAO H., WEI Y., FAN Q., CHEN X., SAVOYE Y., TU C., COHEN-OR D., CHEN B.: Build-to-last: Strength to weight 3d printed objects. *ACM Trans. Graph. (Proc. SIGGRAPH) 33*, 4 (August 2014), 97:1–97:10. doi:10.1145/2601097.2601168. 1

[MDL16] MARTÍNEZ J., DUMAS J., LEFEBVRE S.: Procedural voronoi foams for additive manufacturing. *ACM Trans. Graph. 35*, 4 (July 2016). URL: https://doi.org/10.1145/2897824.2925922, doi:10.1145/2897824.2925922. 1

[Mic04] MICHELL A.: Lviii. the limits of economy of material in frame-structures. *Philosophical Magazine Series 1 8* (1904), 589–597. doi:10.1080/14786440409463229. 1

[MSDL17] MARTÍNEZ J., SONG H., DUMAS J., LEFEBVRE S.: Orthotropic k-nearest foams for additive manufacturing. *ACM Transactions on Graphics 36*, 4 (July 2017), 1–12. doi:10.1145/3072959.3073638. 1

[Pea93] PEARSON J. A.: Complex patterns in a simple system. *Science 261* (1993), 189–192. doi:10.1126/science.261.5118.189. 3

[Ped89] PEDERSEN P.: On optimal orientation of orthotropic materials. *Structural optimization 1* (1989), 101–106. doi:10.1007/BF01637666. 1

[PT08] PANTZ O., TRABELSI K.: A post-treatment of the homogenization method for shape optimization. *SIAM Journal on Control and Optimization 47*, 3 (2008), 1380–1398. doi:10.1137/070688900. 1

[SOG*21] STUTZ F., OLSEN T., GROEN J., AAGE N., SIGMUND O., SOLOMON J., BÆRENTZEN J. A.: Synthesis of frame field-aligned multi-laminar structures. *ArXiv abs/2104.05550* (2021). 1

[SPG19] SCHMIDT M.-P., PEDERSEN C. B., GOUT C.: On structural topology optimization using graded porosity control. *Structural and Multidisciplinary Optimization 60*, 4 (2019), 1437–1453. doi:10.1007/s00158-019-02275-x. 1

[Tur52] TURING A. M.: The chemical basis of morphogenesis. *Philosophical Transactions of the Royal Society of London. Series B, Biological Sciences 237*, 641 (1952), 37–72. doi:10.1098/rstb.1952.0012. 3

[WAWS18] WU J., AAGE N., WESTERMANN R., SIGMUND O.: Infill optimization for additive manufacturing—approaching bone-like porous structures. *IEEE Transactions on Visualization and Computer Graphics 24*, 2 (2018), 1127–1140. doi:10.1109/TVCG.2017.2655523. 1

[Woo60] WOOD L. W.: Relation of strength of wood to duration of load. 1

[WSG21] WU J., SIGMUND O., GROEN J. P.: Topology optimization of multi-scale structures: A review. *Structural and Multidisciplinary Optimization 63* (2021), 1455–1480. doi:10.1007/s00158-021-02881-8. 1

[WWG21] WU J., WANG W., GAO X.: Design and optimization of conforming lattice structures. *IEEE transactions on visualization and computer graphics 27*, 1 (2021), 43–56. doi:10.1109/TVCG.2019.2938946. 4